FIRST STEPS TO YUKON DELTA BIOPHYSICAL MODELING: MONITORING SEA ICE CHANGE USING RECONSTRUCTED NSCAT DATA

Perry J.Hardin[1], Tina Wyllie-Echeverria[1], Sandy Wyllie-Echeverria[2],
Nate Curritt[1], David G. Long[1], and Robert Stehn

ABSTRACT

Within the rich ecological zone of the Bering Sea, researchers have recently recognized the relationship between biophysical parameters such as dates of sea ice retreat and the seasonal habits of several species of both birds and fish, however monitoring these relationships has been difficult due to the large size of the region and the paucity of climatic and oceanic monitoring stations located there. Because of these factors, satellite remote sensing has played an important role in ecological studies of the Bering Sea. Despite their obvious utility, studies of Bering Sea ice have been notoriously challenging for some remote sensing instruments. For example, near infrared and optical sensors that depend on target illumination by the sun cannot be used during the dark near-solstice weeks. Even when illumination is not a problem, dense regional cloud cover accompanying extratropical cyclones that form and pass through the Gulf of Alaska make ice mapping using many instruments successful only in localized cloud-free areas. Because of these limiting factors, active microwave instruments have been found useful for mapping sea ice conditions in the Northern Hemisphere. The project reported in this paper has the ultimate goal of relating sea ice movement to walleye pollock seasonal distributions and nesting locations of several waterbird species. As a report of work in-progress to support that goal, this paper outlines the results of research designed to utilize low cost reconstructed NSCAT imagery for mapping the sea-ice edge in the Bering Sea through the winter of 1996-1997. In summary, simple algorithms applied to reconstructed NSCAT imagery were capable of producing Bering Sea ice edges which agreed closely with those published by the National Ice Center for comparable periods. We believe that reconstructed satellite imagery can play an important future role in the mapping of sea ice as an adjunct to Advanced Very High Resolution Radiometer (AVHRR) and Special Sensor Microwave / Imager (SSM/I) data currently used for the task.

1. INTRODUCTION

The goals of the project reported in this paper follow.

1. To determine whether reconstructed NASA Scatterometer (NSCAT) data can be used to detect and define the seasonal ice edge in the Bering Sea.
2. To compare NSCAT derived sea ice concentration maps with the published weekly ice concentration maps of the National Ice Center (NIC).
3. To compare the sea ice characteristics used in developing a sea ice index (Wyllie-Echeverria and Wooster 1998) with NSCAT derived ice-edge data.

The third goal requires some explanation. The sea ice index is based upon weekly maps (1972-present) from the NIC used to estimate the maximum extent of the seasonal sea ice edge. This index can be used to predict the general environmental conditions of warm or cool on the Bering Sea shelf the following summer. Arctic and sub-arctic populations such as Arctic cod (*Boreogadus saida*) and walleye pollock (*Theragra chalcogramma*) respond to environmental conditions on this scale. Arctic cod are more widespread on the shelf under cool conditions and the subarctic pollock are more restricted than under warm conditions. Since a considerable portion of summer populations on the shelf consist of subarctic species that have migrated northward as seas become ice-free, the

[1] Microwave Earth Remote Sensing Group, 676 SWKT, Brigham Young University, Provo, UT
[2] School of Marine Affairs, University of Washington, Seattle, WA.

* Presented at the Fifth Int'l Conf. on Remote Sensing for Marine and Coastal Environments, San Diego, CA, 5-7 October 1998.

consequences of populations behaving differently with warm or cool conditions is system-wide. NSCAT data may be useful in refining this index.

This report begins with a review of scatterometry and the method of reconstructing low resolution NSCAT imagery to higher resolution. Following that description, a straightforward algorithm useful in defining the sea ice edge from NSCAT data will be presented. We will then present some descriptive statistics and graphs that summarize Bering Sea ice backscatter characteristics and demonstrate how those characteristics change through time. The results of our sea ice detection algorithm will then be discussed. Finally, we will consider the value of the research in the context of future biophysical modeling.

2. DATA

2.1 Scatterometers and Image Reconstruction

Scatterometers are active microwave instruments designed to measure wind velocity and direction over the ocean. Despite this primary mission, scatterometers have also been used to acquire data over land, primarily for instrument calibration purposes. Like its predecessor the Seasat Scatterometer, NSCAT measured backscatter (σ_0) over a wide range of incidence angles, at several azimuth angles, and with both horizontal and vertical polarizations. The wide swath enabled frequent observation of targets. By combining data from multiple passes with the "SIRF" algorithm as described in Long and Hardin (1993, 1994), enhanced resolution images of the surface backscatter were made with an effective resolution of 4-10 km. Primarily, the SIRF algorithm provides images of σ_0 at a 40° incidence angle (***A***). The algorithm also provides an image of the slope of σ_0 versus incidence angle (***B***). The latter is useful in understanding the scattering mechanisms responsible for the observed backscatter and may prove useful for discriminating between various sea and glacier ice types.

Unlike Advanced Very High Resolution Radiometer (AVHRR) imagery which represents the earth at a single moment in time, reconstructed scatterometer imagery gains its resolution enhancement by combining several raw lower resolution images acquired over a period of several days. There is one primary tradeoff in this combination process. As more days of data are combined, the effective resolution of the enhanced image can be improved. On the other hand, events on the image which are dynamic -- phenomena which change the radar backscatter signature over the period of days or weeks used in the combination process -- are not accurately depicted. In this study, NSCAT imagery composites ranged from 3 to 7 days. On the ice-edge maps produced with the composites we were left somewhat puzzled as to what date our final maps of ice edges represented. This confusion may be particularly problematic during the months of spring thaw when the ice edge can change position dramatically from day to day.

Although this report emphasizes results from a single NSCAT compositing period (March 19th – March 25th), there were 14 compositing periods used in the broader study. Of these fourteen, six were picked in-turn for special consideration. Since we had longer-term project goals to do a more complete statistical comparison between AVHRR, SSM/I and NSCAT for sea ice mapping, we chose these six dates because they had relatively cloud-free AVHRR images. A reconstructed NSCAT ***A*** (horizontal polarization) image for the Bering Sea is shown in Figure 1. A NOAA-12 AVHRR Band 4 image is shown for visual comparison in Figure 2.

2.2 NIC Map Product

As described in NIC (1998), the National Ice Center (NIC) began routinely analyzing all marginal ice covered seas since January, 1972. Beginning September, 1996, the product of these analyses has included a twice-weekly sea ice concentration map in GIS format. Typically these digital maps show concentrations ranging anywhere from 30% to 100%. All the NIC weekly regional sea ice maps are the product of a sophisticated analysis utilizing a variety of data sources. Near real-time SSM/I and AVHRR imagery are important remotely sensed components of the analysis. When they are available, timely, and can be integrated rapidly, other data sources include Radarsat imagery, ship and shore station observations, drifting buoy reports, ice model output, and information from foreign ice services. Figure 3 is a generalized sea ice concentration map produced by the National Ice Center for March 18th, 1997. Metadata accompanying the image indicated that AVHRR was the primary source of information for the creation of the map.

3. ANALYSIS

3.1 Exploratory Analysis

Two exploratory analyses were conducted preparatory the actual attempt to discriminate sea ice from ocean water. First, descriptive statistics of backscatter were calculated for the various sea ice classes and water. This description was performed by extracting the NSCAT pixels corresponding to the different NIC classes during each of the six different compositing periods. We did this analysis with hopes we would be able to discriminate not only between ice and water, but between different densities of ice as well. Secondly, we tracked various densities of sea ice through the season to determine whether the average backscatter changed during the time period. For any given density of sea ice, our expectation was that snow depths, ridging, rafting, and the extent of ponded water on the ice would affect the backscatter measured by NSCAT.

3.2 Mapping Sea Ice Edges with NSCAT

A variety of methods are available for mapping sea ice from satellite imagery. However, mapping of sea ice with a scatterometer has a unique challenge – a challenge that arises directly as a result of the scatterometer's primary mission as an instrument to measure ocean wind vectors. Simply speaking, calm water provides little backscatter at the NSCAT Ku-band frequency. However, as ocean winds increase, and waves (and wavelets) grow larger, backscatter amounts approach the high values associated with sea ice. Because of this, the most difficult task with mapping the location of sea ice with NSCAT is to remove the confusion between the bonafide sea ice and the very windy regions of the ocean which have a backscatter nearly identical to sea ice. To solve this problem, Remund and Long (1998) utilize an elegant algorithm predicated on ratios of horizontal to vertical backscatter. In contrast, our approach is much more straightforward.

1. All image pixels corresponding to land are eliminated from consideration.
2. All image pixels south of the Bering Sea continental shelf are isolated in the image. This is done under the assumption that pack ice would never extend south of the Bering Sea continental shelf.
3. The average of all these isolated water pixels is calculated. This is termed the "global average water backscatter value."
4. Each non-land cell in the image is examined in-turn. For the given cell in question, an average backscatter value is calculated from the cell's backscatter value itself and those of its 8-connected cells.
5. If the average value calculated is greater than the global average water backscatter value, the pixel is assumed to be ice, otherwise it is placed in the water category.
6. Any pixel south of the Bering Sea continental shelf is classified as water, regardless of its backscatter.

4. RESULTS AND INTERPRETATION

Figure 4 shows how the average backscatter of various sea ice density classes changes throughout the season. Ice forms initially by the crystallization of water droplets due to the cooling of the sea surface and atmosphere. This new ice is not consolidated, but rather consists of many ice particles grouped together – it becomes grease ice. As the grease ice thickens and collides with other particles it merges into pancake ice and with time these groups of pancake ice consolidate and form solid first-year ice. Compared to later-season ice, this ice is very thin and smooth. However, stresses and movement in the ice from wind cause this thin ice to ridge and raft -- it successively breaks-up and reconsolidates to form a very rough surfaced ice pack (at many scales of analysis). We would expect this sea ice to generate more backscatter. With more time however, the ice takes on a smoother appearance at Ku-band frequencies. Ablation, slow melting, and snowfall will have smoothed the ice at micro-scales although the ice may continue to have the gross hummocky appearance imparted from the earlier rifting and rafting. Finally, the introduction of warmer water at the end of an ice season combined with warmer air temperatures further smooth the ice surface as it melts and the ice edge retreats to the north. Ponding in the ice itself will also lower backscatter. While the graph generally reflects these patterns, there are many anomalies that we cannot currently explain.

Figure 5 represents the sea ice map produced from the March 19th to March 25th, 1997 NSCAT imagery. A visual comparison with the NIC map of the same time period (Figure 3) indicates good agreement. As shown in

Figure 6, the comparison of sea ice extent along longitude 169W matched exactly for 3 dates throughout the 27 week study period but deviated as much as 1.8 degrees (8 January) in the middle of the season. We found the NSCAT and NIC derived data to be within 28 kilometers difference in 40% of the cases. As mentioned in Wyllie-Echeverria and Wooster (1998) the 169th westerly meridian is the line of longitude chosen for the seasonal sea ice index.

5. IMPLICATIONS FOR BIOPHYSICAL MODELING

The usefulness of weekly sea ice edge evaluations has been documented (Wyllie-Echeverria and Wooster 1998). It can be used to predict environmental conditions the following summer. For example, the extent of sea ice is related to the amount of subsurface cold water that is resident in the middle shelf area during summer (Figure 7). This "cold pool" is colder than 2° C and affects the distribution of subarctic species. Future work will focus on individual species responses to cool and warm conditions and how these conditions affect ecosystem dynamics. Concomitant with the strong El Niño of 1997/98 were abnormal conditions on the Bering Sea shelf (Vance *et al.* 1998). Further work is planned, focusing on a suite of commercially important bottomfish species and waterbirds that migrate to the Bering Sea each summer.

The estimated hatch dates for five species of geese show a trend toward earlier dates over the past 16 years (Bowman *et al.*, 1997). All species have earlier average estimated hatch dates. Earlier hatch dates are correlated to how long the seasonal sea ice remains over the middle shelf area ($r = 0.4$; $p > 0.05$). This ice condition may affect how early the birds are able to migrate to their preferred nesting sites on the Yukon Delta. Furthermore, hatch dates are significantly correlated to sea level pressure in May ($r = 0.70$; $P > 0.05$) which has been lower in recent years too. We plan to evaluate changes in nesting sites over the 16 year data set to see if location has changed along with hatch dates.

Spring ice conditions during April and May may be a critical time in setting up conditions on the Bering Sea shelf that will persist throughout summer. The annual extent of sea ice is significantly correlated to the direction of wind toward the shelf during April (Wyllie-Echeverria and Wooster 1998) and is an integral component of the sea ice index. More analysis is necessary to establish environmental links with the biological component of the Bering Sea system. We plan to continue evaluating remotely sensed data in an effort to characterize the key physical components affecting the biological components on the shelf.

6. CONCLUSIONS

Given these preliminary results, we consider NSCAT and future scatterometers to be important contributors to Bering Sea ice mapping. While scatterometry may never displace AVHRR and SSM/I, reconstructed scatterometry clearly has a future role as an adjunct data source. Given that many biological studies hinge on accurate maps of sea ice retreat and formation, future refinement in sea ice mapping with scatterometry is warranted.

7. ACKNOWLDGEMENTS

The authors gratefully acknowledge the generous funding of this project by the National Science Foundation.

8. REFERENCES

Bowman, T., R. Stehn, M. Wege and G. Walters. (1997). Populaiton size and production of geese and eiders nesting on the Yukon-Kuskokwim Delta, AK in 1997. *U.S. Fish and Wildlife Service Field Report*. Anchorage, AK 99503. p.22.

Long, D.G. and P.J. Hardin (1993) High resolution imaging of land/ice using spaceborne scatterometry part I: the imaging technique. *IEEE Transactions on Geoscience and Remote Sensing*. Vol. 31, No. 3, pp. 700-715.

Long, D.G. and P.J. Hardin (1994) High resolution imaging of land/ice using spaceborne scatterometry part II: vegetation studies of the Amazon and future applications. *IEEE Transactions on Geoscience and Remote Sensing*. Vol . 32, No. 2, pp. 449-460.

National Ice Center (1998). West Arctic Web Page. *http://www.natice.noaa.gov/index.htm*

Remund, Q. P. and D. G. Long. (1998). Sea-Ice extent mapping using Ku-band scatterometer data. *J. Geophys. Res.* In press.

Vance, T., C. T. Baier, R. D. Brodeur, K. O. Coyle, M. B. Decker, G. L. Hunt, Jr., J. M. Napp, J. D. Schumacher, P. J. Stabeno, D. Stockwell, C. T. Tynan, T. E. Whitledge, T. Wyllie-Echeverria, and S. Zeeman. (1998). Anomalies in the Ecosystem of the Eastern Bering Sea:Including Blooms, Birds and other Biota. *Eos, Trans. Amer. Geophys Union* 79:121, 126.

Wyllie-Echeverria, T. and W. Wooster. (1998). Variations in Sea Ice and the Cold Pool of the Bering Shelf: Consequences to the ecosystem. *Fisheries Oceanography*. In Press.

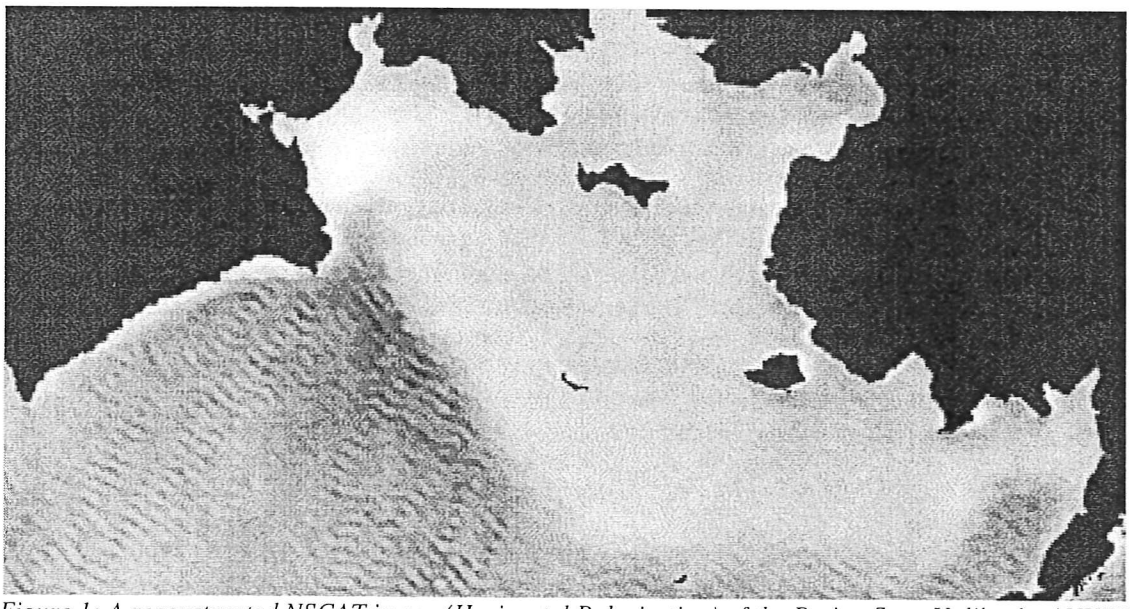

Figure 1: A reconstructed NSCAT image (Horizontal Polarization) of the Bering Sea. Unlike the AVHRR image of Figure 2 which represents a moment in time, this image was constructed from lower resolution NSCAT imagery during the time period from March 19th to March 25th, 1997

Figure 2: A Band 4 NOAA-12 AVHRR image of the Bering Sea. The image was acquired March 24,1997

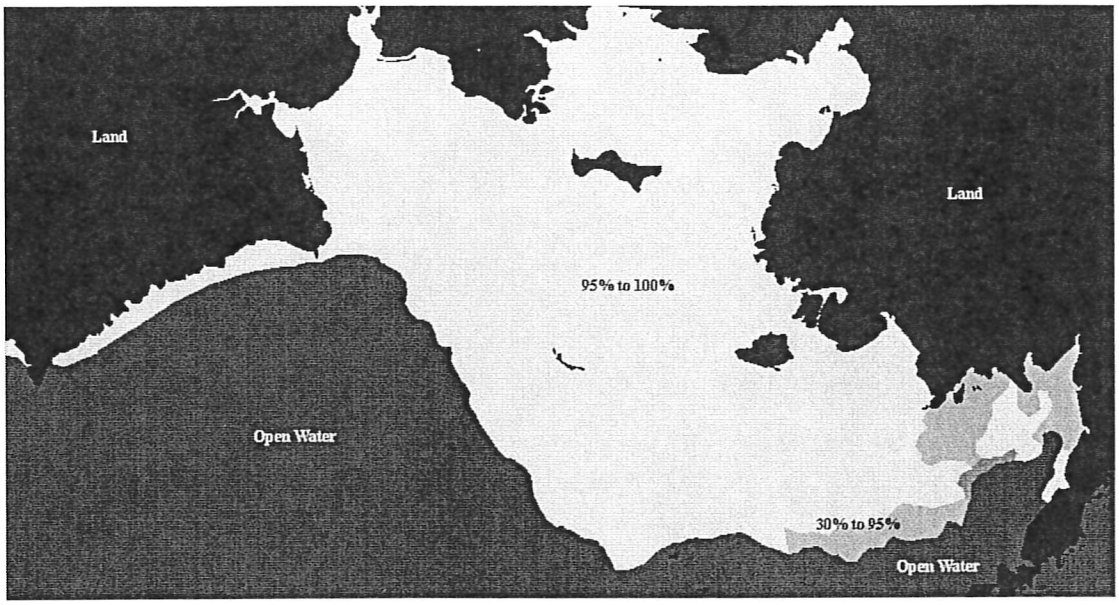

Figure 3. The NIC sea ice concentration map for March 18th, 1997. The shades of gray are inversely proportional to the concentration of sea ice.

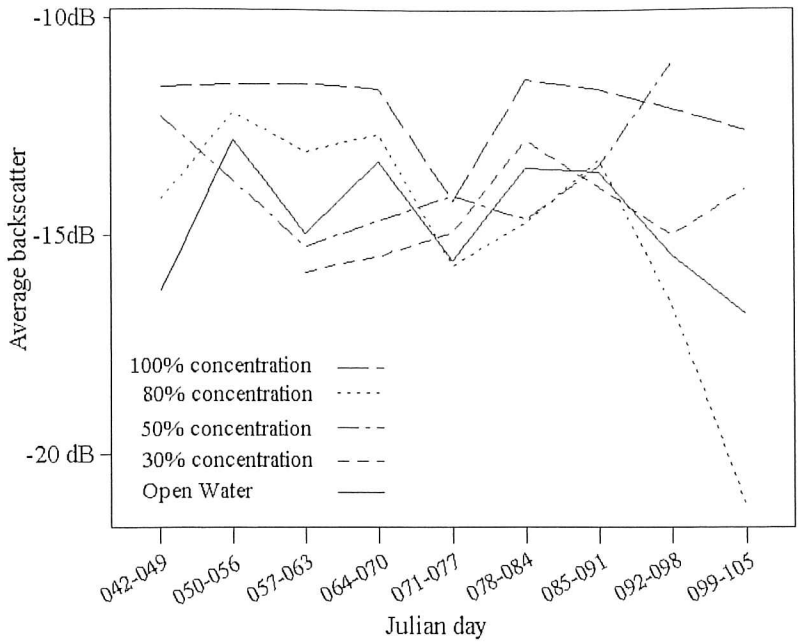

Figure 4. Mean backscatter for the different ice concentrations follow the general pattern theory would suggest, with some admitted anomalies.

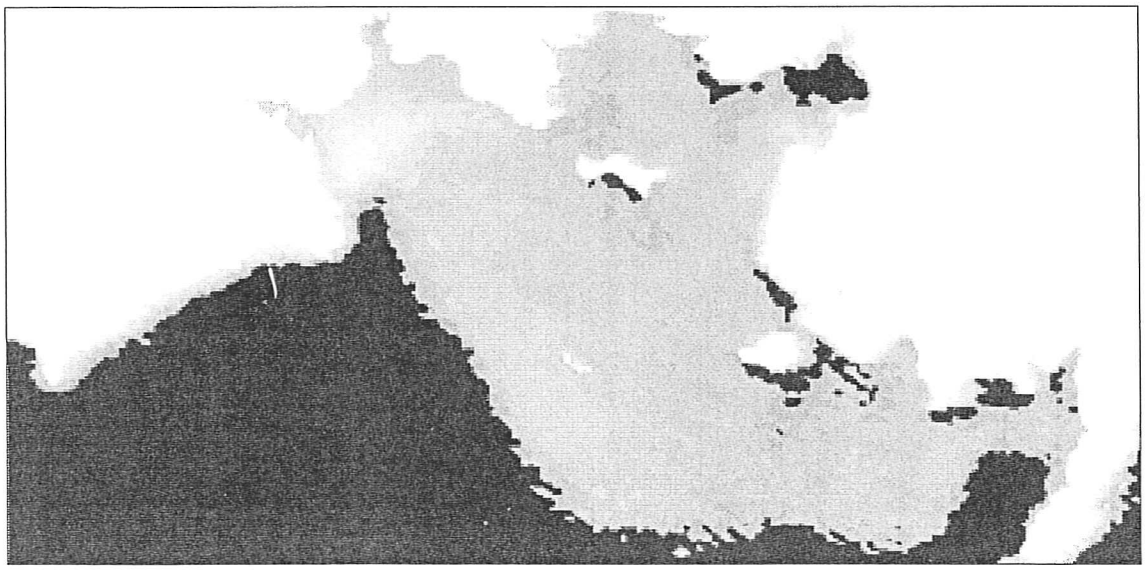

Figure 5. The NSCAT-based sea ice map produced from the March 19th to March 25th, 1997 scatterometry. A visual comparison with the NIC map of the same time period (Figure 3) indicates good general agreement.

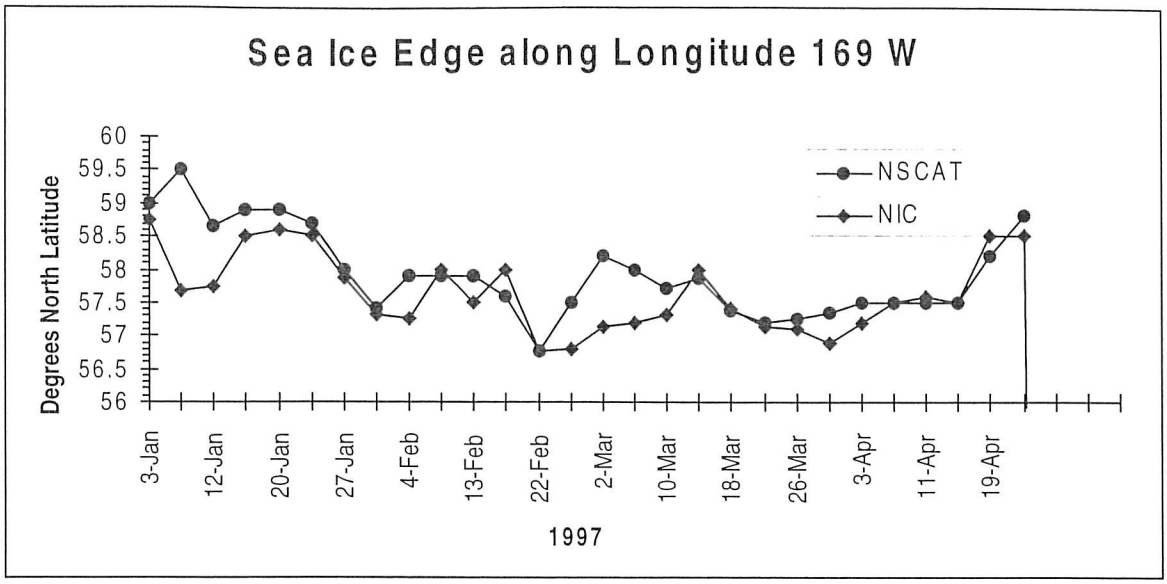

Figure 6. A graph of the sea ice edge location along the 169th westerly meridian. Although there is good general agreement most of the season, the most severe deviation is nearly 200 kilometers. The average difference is approximately 28 kilometers.

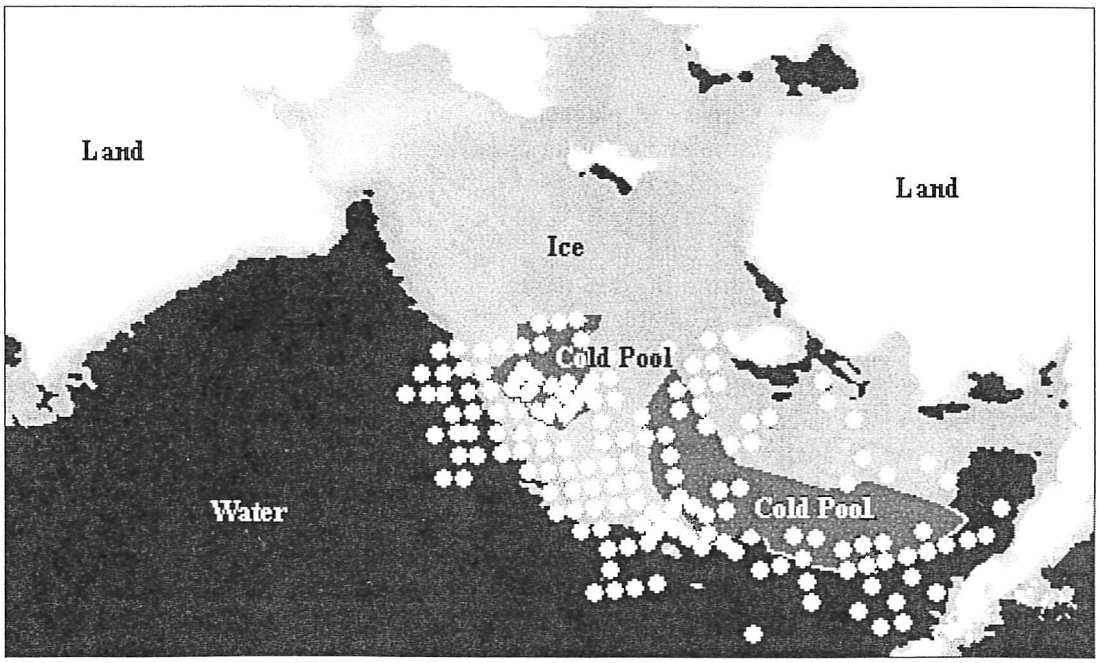

Figure 7. A comparison of the sea ice map produced using reconstructed NSCAT with the location of the cold pool and pollock schools. Pollock schools are shown as white dots.